

# Saturation of Zeldovich Stretch-Twist-Fold Map Dynamos

AMIT SETA<sup>1,2</sup> †, PALLAVI BHAT<sup>3</sup>  
AND KANDASWAMY SUBRAMANIAN<sup>3</sup>

<sup>1</sup>UM-DAE Center For Excellence in Basic Sciences, University of Mumbai, Vidyanagari  
Campus, Mumbai 400098, India

<sup>2</sup>School of Mathematics & Statistics, Newcastle University, Newcastle upon Tyne NE1 7RU,  
UK.

<sup>3</sup>IUCAA, Post Bag 4, Ganeshkhind, Pune 411 007, India.

(Received 7 July 2021)

Zeldovich’s stretch-twist fold (STF) dynamo provided a breakthrough in conceptual understanding of fast dynamos, including the small scale fluctuation dynamos. We study the evolution and saturation behaviour of two types of generalized Baker’s map dynamos, which have been used to model Zeldovich’s STF dynamo process. Using such maps allows one to analyze dynamos at much higher magnetic Reynolds numbers  $R_M$  as compared to direct numerical simulations. In the 2-strip map dynamo there is constant constructive folding while the 4-strip map dynamo also allows the possibility of a destructive reversal of the field. Incorporating a diffusive step parameterised by  $R_M$  into the map, we find that the magnetic field  $B(x)$  is amplified only above a critical  $R_M = R_{\text{crit}} \sim 4$  for both types of dynamos. The growing  $B(x)$  approaches a shape invariant eigenfunction independent of initial conditions, whose fine structure increases with increasing  $R_M$ . Its power spectrum  $M(k)$  displays sharp peaks reflecting the fractal nature of  $B(x)$  above the diffusive scale. We explore the saturation of these dynamos in three ways; via a renormalized reduced effective  $R_M$  (Case I) or due to a decrease in the efficiency of the field amplification by stretching, without changing the map (Case IIa), or changing the map (Case IIb), and a combination of both effects (Case III). For Case I, we show that  $B(x)$  in the saturated state, for both types of maps, approaches the marginal eigenfunction, which is obtained for  $R_M = R_{\text{crit}}$  independent of the initial  $R_M = R_{M0}$ . On the other hand in Case II, for the 2-strip map, we show that  $B(x)$  saturates preserving the structure of the kinematic eigenfunction. Thus the energy is transferred to larger scales in Case I but remains at the smallest resistive scales in Case II as can be seen from both  $B(x)$  and  $M(k)$ . For the 4-strip map,  $B(x)$  oscillates with time, although with a structure similar to the kinematic eigenfunction. Interestingly, the saturated state in Case III shows an intermediate behaviour, with  $B(x)$  similar to the kinematic eigenfunction at an intermediate  $R_M = R_{\text{sat}}$ , with  $R_{M0} > R_{\text{sat}} > R_{\text{crit}}$ .  $R_{\text{sat}}$  is determined by the relative importance of the increased diffusion versus the reduced stretching. These saturation properties are akin to the range of possibilities that have been discussed in the context of fluctuation dynamos.

## 1. Introduction

Magnetic fields in astrophysical systems are thought to arise by amplification of a seed magnetic field by dynamo action. In this process kinetic energy of motions is converted to magnetic energy. A generic dynamo is the small-scale or fluctuation dynamo, which arises in any random or turbulent flow (Kazantsev 1968; Zeldovich *et al.*

† Email address for correspondence: amitseta90@gmail.com

1983, 1990; Haugen *et al.* 2004; Schekochihin *et al.* 2004; Brandenburg & Subramanian 2005; Tobias *et al.* 2011; Brandenburg *et al.* 2012; Bhat & Subramanian 2014). It is well known that when magnetic Reynolds number  $R_M$  of such a flow is above a certain critical threshold  $R_{\text{crit}} \sim 100$ , the magnetic field in the fluid is amplified rapidly on the eddy turn over time-scales. This amplification is due to the random stretching by the velocity shear. Such shearing motions also lead to the magnetic field developing smaller and smaller spatial scales, until resistive diffusion becomes important to balance the growth. The field then becomes highly intermittent (Zeldovich *et al.* 1990) with the kinematic eigenfunction having power peaked on the resistive scales (Kazantsev 1968). For a random flow driven on a (single) scale  $l$ , the resistive scale is  $l_\eta \sim l/R_M^{1/2}$ , and for  $R_M \gg 1$ , it is much smaller than the driving scale  $l$ . Eventually the Lorentz force of the growing magnetic field provides a back reaction to the dynamo action, leading to the saturation of magnetic field growth. The nature and spatial coherence of the field in the saturated state is of paramount importance to the observational signatures of this field in different astrophysical systems (Subramanian *et al.* 2006; Enßlin & Vogt 2006; Schekochihin & Cowley 2006; Bhat & Subramanian 2013), but is however not well understood at present (Brandenburg & Subramanian 2005; Tobias *et al.* 2011; Brandenburg *et al.* 2012).

Indeed there is considerable evidence for magnetic fields in several systems like galaxy clusters (Clarke *et al.* 2001; Clarke 2004) and in young galaxies (Bernet *et al.* 2008) from observations of Faraday rotation that these systems induce on background polarized sources. A possible origin of these fields is the fluctuation dynamo action. However, whether one can indeed reproduce the observed levels of Faraday rotation measure (FRM) depends on the spatial coherence of the fields produced by the fluctuation dynamo. As these systems have typically  $R_M \gg 1$ , the field needs to become much more coherent in the saturated state than it is at the kinematic stage for it to explain the observations (Bhat & Subramanian 2013).

The saturation of fluctuation dynamos has been studied via both direct numerical simulations (DNS) and some simple analytical models. A simple model of Subramanian (1999) suggests that the dynamo can saturate by the Lorentz force driving the dynamo to its marginal state. In such a case the magnetic field in the saturated state concentrates on scales  $l_c \sim l/R_{\text{crit}}^{1/2}$ . As  $R_{\text{crit}} \ll R_M$  typically, this implies a much more coherent field in the saturated state of the dynamo than during the kinematic stage. Using DNS with large magnetic Prandtl numbers ( $P_M = R_M/\text{Re} \gg 1$ ), but small fluid Reynolds numbers ( $\text{Re}$ ), Schekochihin *et al.* (2004) argued that the fluctuation dynamo saturates with the magnetic field still concentrated on resistive scales. On other hand simulations of Haugen *et al.* (2003, 2004) and Eyink *et al.* (2013) with  $P_M = 1$  and a large  $R_M = \text{Re} \approx 10^3$ , found that the magnetic integral scale is just a modest fraction of the velocity integral scale, and much larger than the resistive scale. One could then expect significant FRMs, as is also consistent with the theoretical expectation from Subramanian (1999) and the DNS results of Subramanian *et al.* (2006); Cho & Ryu (2009); Bhat & Subramanian (2013). The case when both  $\text{Re}$  and  $P_M$  are large, as in galactic and cluster plasmas, is of course not easy to simulate and the saturation of the fluctuation dynamo could be quite different (Eyink 2011).

Note that DNS are limited by the  $R_M$  that are achievable and still perhaps do not have a large enough  $R_M$  to unambiguously determine the saturated state. At the same time the analytical models are still rather simplistic. In this context one may wonder if there is any other independent and simple way of studying the generic saturation properties of fluctuation dynamos. We consider here map dynamos that have been studied earlier to

mimic kinematic fast dynamo action, and examine how such maps could saturate. Such map dynamos typically lead to a fractal structure of the field, where the field goes into smaller and smaller scales (Finn & Ott 1988, 1990; Childress & Gilbert 1995). However with the incorporation of a diffusive step in the map, they can lead to eigenfunctions which preserve their shape, and have the smallest scale determined by the resistivity (or the effective  $R_M$ ). In the case of such map dynamos one can reach much larger  $R_M$  than for the case of DNS. We then examine simple models of saturating the map dynamo and study how the spatial structure of the map eigenfunction changes from the kinematic to the saturated state. Our aim is then to get insight into generic properties of the saturated states of the fluctuation dynamo itself.

In the next section we begin with the description of the standard Stretch-Twist-Fold (STF) dynamo (Vainshtein & Zel'dovich 1972). The corresponding map model for the STF dynamo is outlined in section 3. Results from numerical simulation of the STF map dynamo for various  $R_M$  are given in section 4. The saturation of the STF map dynamos is taken up in section 5. The last section presents a discussion of the results and our conclusions.

## 2. Zeldovich's STF dynamo

To explain the possibility of the fast dynamos i.e. growth of magnetic field even when resistivity tends to zero, Vainshtein & Zel'dovich (1972) put forward a heuristic description referred to as 'Stretch-Twist-Fold' (STF) dynamo. The algorithm involves first stretching a closed flux tube to double its length (see for example Fig. 4.6 in Brandenburg & Subramanian (2005)) preserving its volume (a characteristic of an incompressible flow). Assuming magnetic flux to be frozen in the fluid, the magnetic field doubles as the area of the cross-section goes down by a factor of two. Next, the flux tube is twisted into a figure eight and then folded so the direction of magnetic field is same in both sub-parts. Then both parts are merged together into one through small diffusive effects to occupy the same volume as the starting flux tube. A weak diffusion is thus required to make the process of merging irreversible by smoothing region between the two flux tubes during joining without much loss in the flux or energy. †

It may thus be more appropriate to refer to this process as the Stretch-Twist-Fold-Merge dynamo, although we continue with the standard terminology here.

Hence, the final flux tube becomes equivalent to the original single flux tube, but with a field that is double the initial field. It is important to mark the way the two parts are folded: if they are folded with fields pointing in opposite directions it would lead to the cancellation of the field and can model the field reversals due to turbulence in the actual physical situation. For a constructive folding, with each step the flux and thus the magnetic field increases by a factor of 2, repeating the same process  $n$  times the magnetic field increases by a factor of  $2^n$ . Thus the growth rate is  $\sim T^{-1} \ln 2$  where  $T$  is the time for one STF step. The stretching can also be done in a non-uniform manner. Suppose the stretching is done non-uniformly, by stretching a fraction  $\beta$  (where  $0 < \beta < 1/2$ ) of the circumference ( $2\pi R$ ) by an amount  $1/\beta$  and the remaining length  $2\pi\alpha R$  of the circumference by  $1/\alpha$  (where  $\alpha = 1 - \beta$ ). Then this would give rise to the same growth

† Note that diffusion is not essential for the process of amplification of magnetic field in the STF dynamo. Even in random flows where both constructive and destructive twisting and folding are possible, the probability of constructive effect dominates and leads to field amplification (Zeldovich *et al.* 1990; Molchanov *et al.* 1984). However without the diffusion, the map is in principle reversible, so that one can restore the previous state. This is not possible after the diffusive step. Of course diffusion is also required to develop an eigenfunction of the STF dynamo.

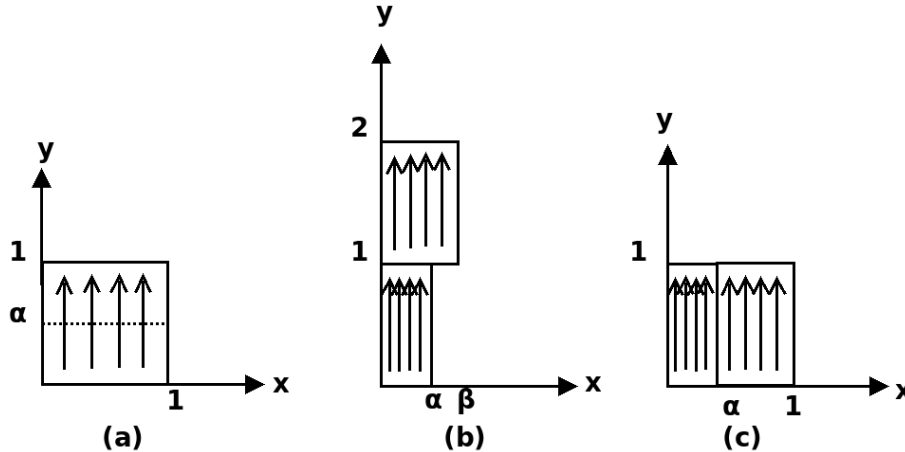


FIGURE 1. The two-dimensional Baker's map as a model for the stretch-twist-fold dynamo, but with non-uniform stretching.

rate in magnetic field as before but in a non-uniform way. Repeated operation of the inhomogeneous STF process on a flux tube or on one that has developed reversals, would lead to the magnetic field developing a fine scale structure that can mimic the intermittent nature of the field generated by fluctuating dynamos.

### 3. Map Models for Zeldovich's STF Dynamos

Finn & Ott (1988, 1990) studied a map analogue of Zeldovich's Stretch-Twist-Fold fast dynamo. Fig.3 represents the two-dimensional map which is used to model the dynamo. This map is an example of the generalised Baker's map (Childress & Gilbert 1995). We begin with a perfectly conducting two-dimensional square sheet in the  $(x, y)$  plane, and a uniform upward (or  $y$ ) directed seed magnetic field of say a unit strength. The magnetic field initially, and at all times is independent of  $y$  (analogous to being independent of the toroidal direction in a flux tube). Now, the lower part of the square ( $0 < y < \alpha$ ) is horizontally compressed by a factor  $\alpha$  and, to conserve the area simultaneously stretched vertically by factor  $1/\alpha$ . Similarly, the upper part ( $\alpha < y < 1$ ) is compressed by factor  $\beta$  (along  $x$ ) and stretched by factor  $1/\beta$  (along  $y$ ) where  $\beta = 1 - \alpha$ . Then the two parts are separated, the magnetic field between the two parts is cut and the two pieces are rearranged to get back the original square. (This non-physical action allows one to describe an inherently three-dimensional physical process by a two-dimensional map; there cannot be any dynamo action in two-dimensional flows (Zeldovich *et al.* 1983)). As the flux is frozen in the region ( $\eta \rightarrow 0$ ), the field through the  $\alpha$  strip,  $B_\alpha$  increases to  $B/\alpha$  and the field through the  $\beta$  strip,  $B_\beta$  by  $B/\beta$ , where  $B = 1$  is the initial field. Then the total flux is  $B\alpha + B\beta = 2$ , and thus the flux through entire square doubles. The average magnetic field also doubles within the square as compared to the initial field.

The map that captures the above process is as follows:

$$x_{n+1} = \begin{cases} \alpha x_n & : y_n < \alpha; \\ \beta x_n + \alpha & : y_n > \alpha; \end{cases} \quad (3.1)$$

$$y_{n+1} = \begin{cases} y_n/\alpha & : y_n < \alpha; \\ (y_n - \alpha)/\beta & : y_n > \alpha; \end{cases} \quad (3.2)$$

Note that  $x_n$  and  $y_n$  take values in the interval  $[0, 1]$ . The corresponding amplification of

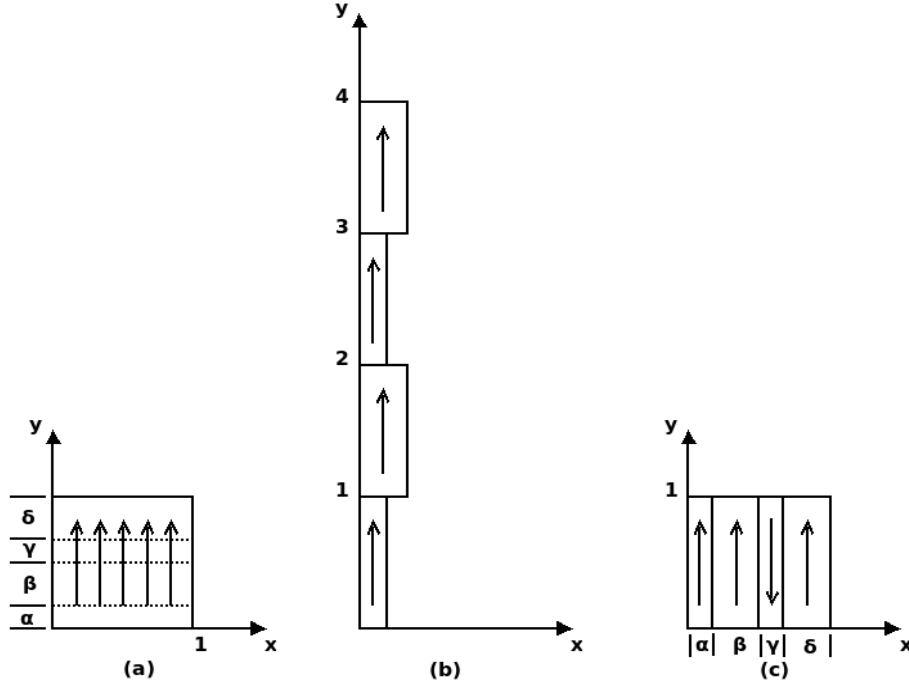


FIGURE 2. The two-dimensional 4-strip Baker's map as a model for the stretch-twist-fold dynamo with cancellation of fields.

magnetic field in the region is given as:

$$B_{n+1}(x_{n+1}) = \begin{cases} B_n(x_n)/\alpha & : x_n < \alpha; \\ B_n(x_n)/\beta & : x_n > \alpha; \end{cases} \quad (3.3)$$

### 3.1. Amplification, cancellation and the four-strip map

To include field reversals, which are an important part of the physical dynamo process leading to cancellation of magnetic fields, Finn & Ott (1988, 1990) suggest a different model for STF dynamos. The flux tube in this case is stretched non-uniformly to four times its original circumference, twisted in to four loops, and two of the loops are folded with the same orientation of magnetic field while the other two with the opposite directions of fields thus leading to a partial field cancellation. The corresponding map is shown in Fig. 2. The net field increase is same as in the two-strip map, the field doubles with each step. As shown in the Fig. 2, the analogous map would involve dividing the square into four strips and while rearranging the strips, one of them is inverted and then placed to regain the initial square configuration. The analytical description of the four-strip map is given by-

$$x_{n+1} = \begin{cases} \alpha x_n & : y_n < \alpha; \\ \beta x_n + \alpha & : \alpha < y_n < (\alpha + \beta); \\ \gamma(1 - x_n) + \alpha + \beta & : (\alpha + \beta) < y_n < (\alpha + \beta + \gamma); \\ \delta x_n + \alpha + \beta + \gamma & : (\alpha + \beta + \gamma) < y_n < 1; \end{cases} \quad (3.4)$$

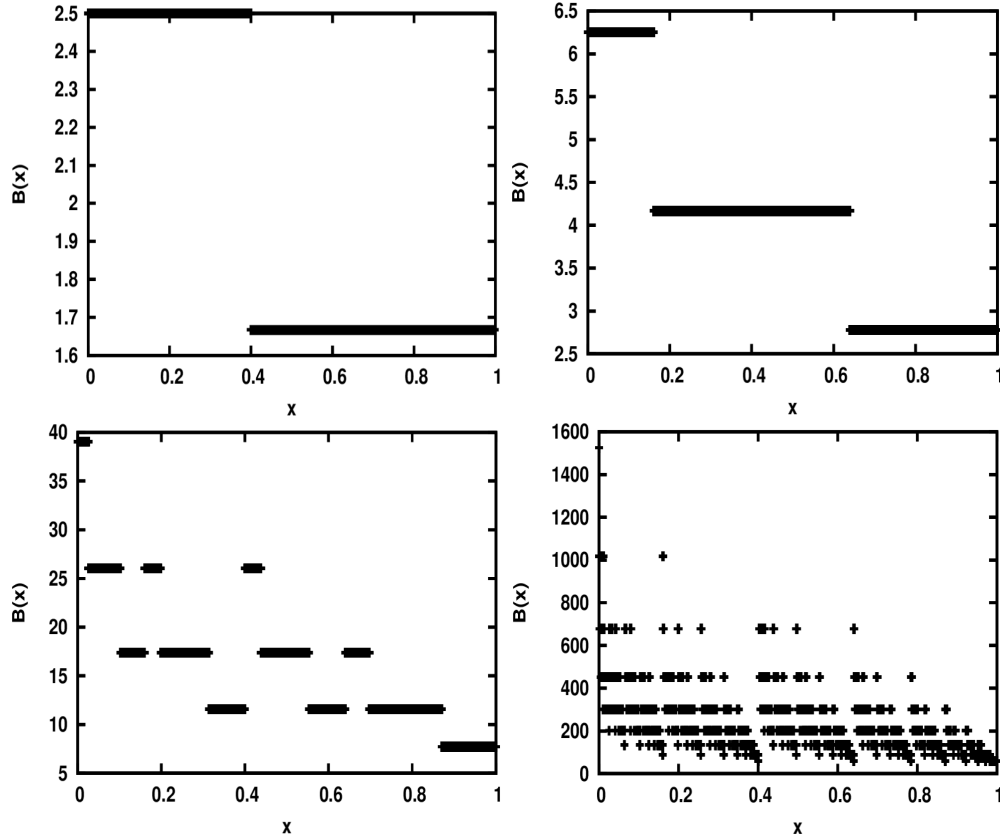


FIGURE 3. Magnetic field evolution in the two-strip map with  $\alpha = 0.4$  after 1, 2, 4 and 8 iterations (top left to bottom right panels). The magnetic field strength  $B(x)$  is given in the units of the seed field. We see the amplification of the field strength and development of the intermittent structure of the field as the number of iterations increases.

$$y_{n+1} = \begin{cases} y_n/\alpha & : y_n < \alpha; \\ (y_n - \alpha)/\beta & : \alpha < y_n < (\alpha + \beta); \\ ((\alpha + \beta + \gamma) - y_n)/\gamma & : (\alpha + \beta) < y_n < (\alpha + \beta + \gamma); \\ (y_n - (\alpha + \beta + \gamma))/\delta & : (\alpha + \beta + \gamma) < y_n < 1; \end{cases} \quad (3.5)$$

Again  $x_n$  and  $y_n$  take values in the interval  $[0, 1]$ . The corresponding amplification of magnetic field with a flip of sign in the third strip is now given by:

$$B_{n+1}(x_{n+1}) = \begin{cases} B_n(x_n)/\alpha & : y_n < \alpha; \\ B_n(x_n)/\beta & : \alpha < y_n < (\alpha + \beta); \\ -B_n(x_n)/\gamma & : (\alpha + \beta) < y_n < (\alpha + \beta + \gamma); \\ B_n(x_n)/\delta & : (\alpha + \beta + \gamma) < y_n < 1; \end{cases} \quad (3.6)$$

We will study both two-strip and four-strip maps in what follows.

### 3.2. Magnetic Diffusion

As discussed above, it is important to include the smoothing effect of diffusion in the STF dynamo. We do this in the maps by convolving the evolved magnetic field after each step with a Gaussian. If  $T$  is the time interval for each complete cycle of the STF map, the assumption is that for the time  $T/2$  the diffusive term in the induction equation can be neglected, the flux is frozen and the field amplifies. For the remaining period,  $T/2$ ,

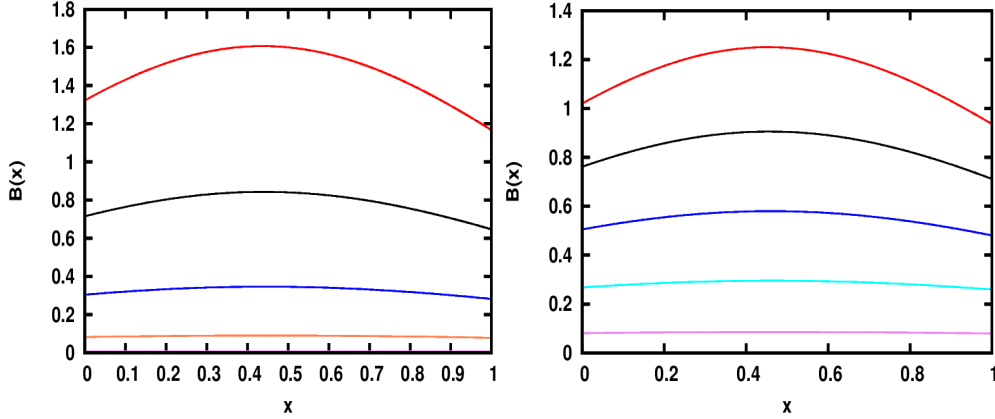


FIGURE 4.  $B(x)$  for the two-strip map (left panel) and for the four-strip map (right panel) including diffusion, after 8 iterations. In the left panel the curves from bottom to top correspond to values of  $R_M = 2, 3, 4, 5$  respectively, while in the right panel they correspond to  $R_M = 1, 2, 3, 4, 5$ . The field is amplified for a critical magnetic Reynolds number  $R_{\text{crit}} \gtrsim 4$  in both cases.

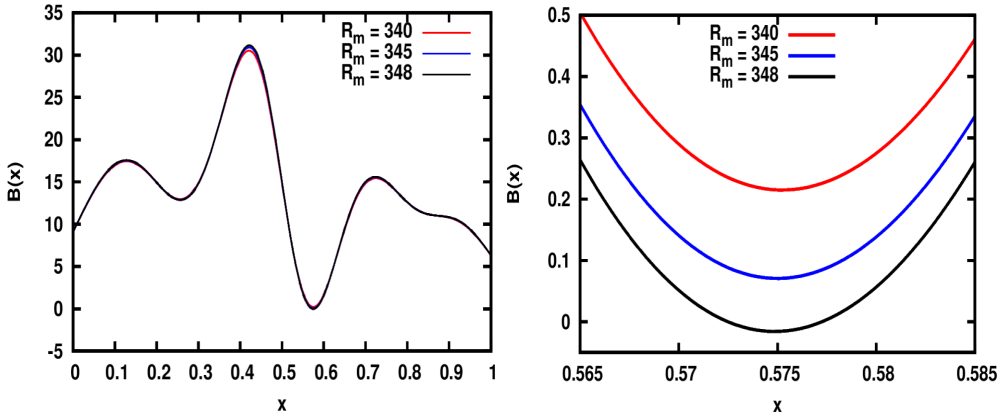


FIGURE 5. Left-hand panel:  $B(x)$  for the four-strip map after 4 iterations, with the darkest curve corresponding to  $R_M = 348$ . A magnified version is shown in the right panel.  $B(x)$  becomes negative first for  $R_M \sim 348$ , depending on the stretching parameters. Here we have adopted  $\alpha = \delta = 7/16$  and  $\beta = \gamma = 1/16$ .

the advection term vanishes and diffusion acts, with twice the normal diffusivity. The magnetic Reynolds number  $R_M$  is the measure of advection in comparison to diffusion and thus should be a parameter in the convolving function. The convolving Gaussian (also the Green's function for diffusion) is therefore taken as (Finn & Ott 1990),

$$G(x, x') = (R_M/4\pi T)^{1/2} \exp[-(x - x')^2 (R_M/4T)]. \quad (3.7)$$

The width of the Gaussian ( $\sigma = \sqrt{2T/R_M}$ ) is inversely proportional to  $\sqrt{R_M}$  and shows that the diffusion diminishes when  $R_M$  increases and viceversa. A single iteration involves applying the map to amplify the magnetic field and then convolving the evolved field with the above Gaussian.

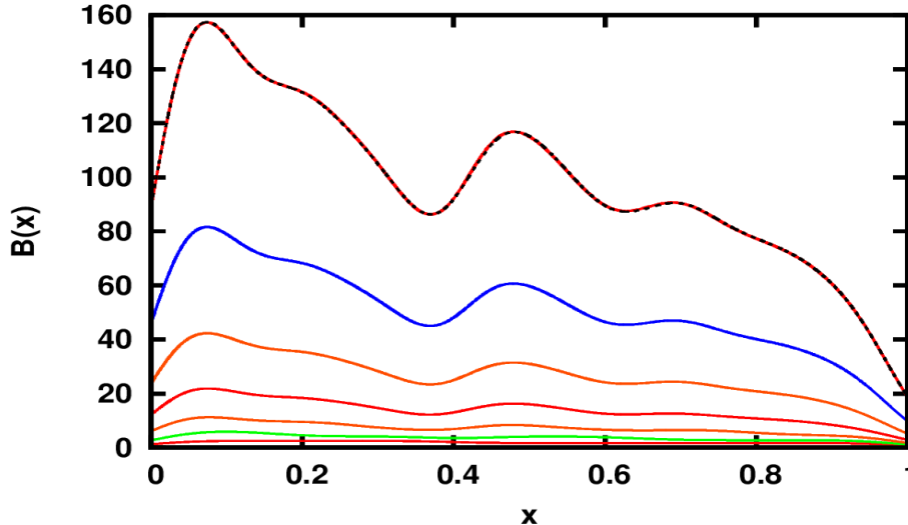


FIGURE 6.  $B(x)$  for the 2-strip map for iterations 1 to 7 (from bottom to top), adopting  $\alpha = 0.4$  and  $R_M = 1000$ .  $B(x)$  after the 7th iteration is just a scaled version of  $B(x)$  after the 6th one illustrating the development of the map eigenfunction.

#### 4. Results: Kinematic Stage

We have coded the amplification of the magnetic field using maps given in Eq. (5.3)-(3.6) and also included diffusion using the set of points in the unit square in the  $(x, y)$  plane. The positions of the points are evolved using the map equations. The distribution of points in the interval  $[0, 1]$  is dynamic and the map automatically allocates more points to areas where the magnetic field has finer structure. This allows us to achieve higher  $R_M$  than the number of points that are used. We have generally adopted  $300 \times 300$  points for lower  $R_M$  runs while for higher  $R_M$  we use  $500 \times 500$  points.

We first show in Fig. 3, the result of applying the two strip map, excluding diffusion to explore kinematic evolution of magnetic field starting from a unit seed field. Fig. 3 shows the magnetic field  $B(x)$ , as a function of position  $x$ , after 1, 2, 4 and 8 iterations. We have adopted  $\alpha = 0.4$ . It is clear from Fig. 3 that as the number of iterations increases magnetic field grows but becomes more and more intermittent. Moreover, within a small spatial scale the magnetic field varies significantly and develops a fractal structure (Finn & Ott 1988, 1990).

##### 4.1. Critical magnetic Reynolds number

In the presence of diffusion, the amplification has to win over it for the net amplification to occur. This introduces a critical  $R_M = R_{\text{crit}}$ , only above which the net amplification takes place. We show in Fig. 4 (left panel) that starting with an initial seed field of 1,  $B(x)$  is not amplified unless  $R_M > R_{\text{crit}}$ . The critical magnetic Reynolds number for the two-strip map is  $R_{\text{crit}} \approx 4.35$ .

We have also incorporated diffusion into the four-strip map with cancellation adopting  $\alpha = \delta = 7/16$  and  $\beta = \gamma = 1/16$ . The results which are shown in Fig. 5 (right panel) suggest a critical magnetic Reynolds number which is very close to that obtained for the two-strip map.

It is interesting to note that, in the four-strip map, where the magnetic field of both polarities are amplified, there is no field with negative polarity in the solution till a large enough  $R_M$  is reached. This critical  $R_M$  of course depends on the stretching parameters,



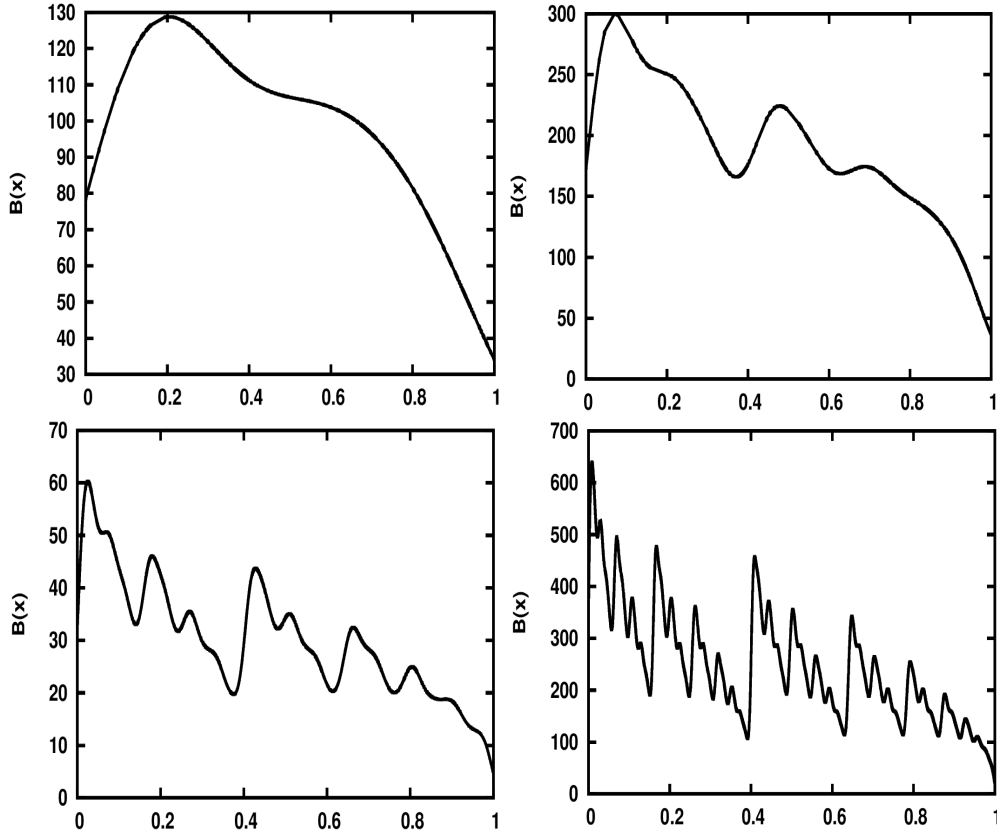


FIGURE 7. Eigenfunctions for the 2-strip map with  $\alpha = 0.4$  and for  $R_M = 100, 1000, 10^4, 10^5$  (top left to bottom right panels).

in particular the value of  $\gamma$ , which determines the degree of amplification of the negative field. As shown in Fig. 5, the field in the region has negative polarity solutions only for  $R_M \gtrsim 348$  for  $\alpha = \delta = 7/16$  and  $\beta = \gamma = 1/16$ .

#### 4.2. Eigenfunctions of the map dynamo

After a few iterations, the function  $B(x)$  representing variation of magnetic field along  $x$  settles to an eigenfunction of a specific shape and  $B(x)$  from future iterations can be matched to it by scaling. This can be seen in Fig. 6 for the two-strip map. For example  $B(x)$  after the 7th iteration can be scaled back in amplitude to  $B(x)$  after the 6th iteration. Thus  $B(x)$  tends to an eigenfunction of the map with diffusion included (which represents the STF dynamo). The eigenfunction of the two-strip map depends of course on  $R_M$ .

This is clear from Fig. 7: the eigenfunction of the magnetic field develops a finer and finer structures with increasing  $R_M$  (from  $10^2$  to  $10^5$ ). The eigenfunctions shown in Fig. 7 for different values of  $R_M$  match those in Fig. 6 of Finn & Ott (1990) for the same  $\alpha = 0.4$ . The eigenfunctions for the four-strip map with  $R_M$  ranging from  $10^2$  to  $10^5$  are shown in Fig. 8. Besides showing features similar to the two-strip maps, the eigenfunctions of the four-strip map have fine-scale reversals of magnetic field. These could be thought of as an analogue of the field reversals seen in the DNS of fluctuation dynamos (Schekochihin *et al.* 2004; Brandenburg & Subramanian 2005).

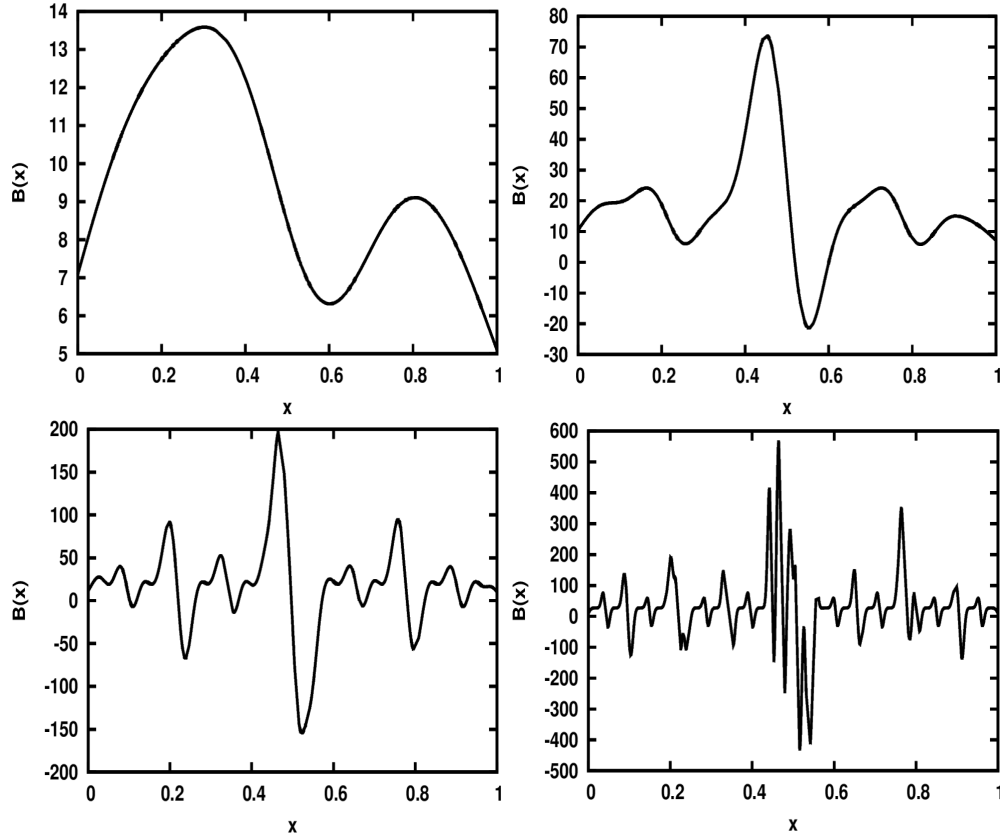


FIGURE 8. Eigenfunctions for the 4-strip map for  $R_M = 100, 1000, 10^4, 10^5$  (top left to bottom right panels). We have adopted  $\alpha = \delta = 7/16$  and  $\beta = \gamma = 1/16$ .

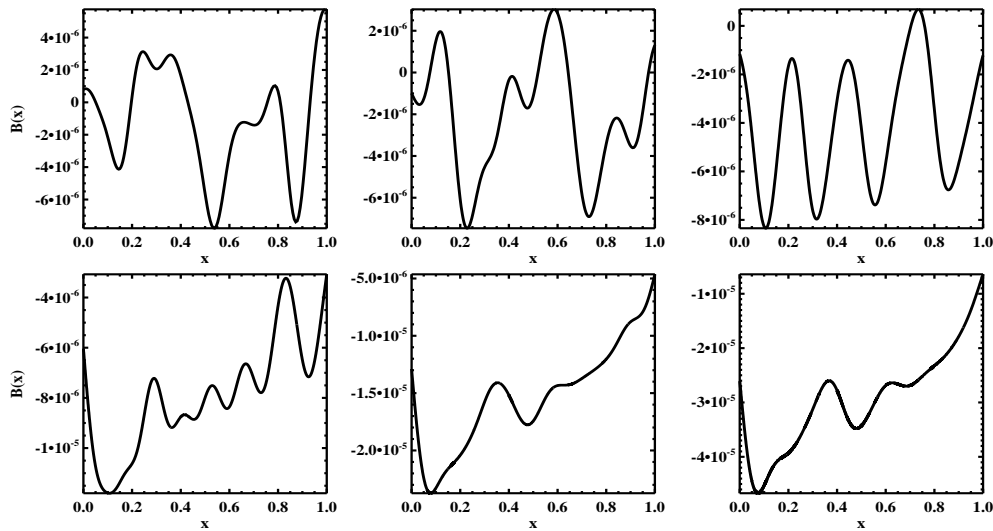


FIGURE 9.  $B(x)$  evolution starting from a random initial seed field, for  $R_M = 1000$ . The iteration number increases from top left to bottom right. The  $B(x)$  in the bottom rightmost panel is the same eigenfunction as  $Rm = 1000$  case is Fig. 7, but with a negative amplitude

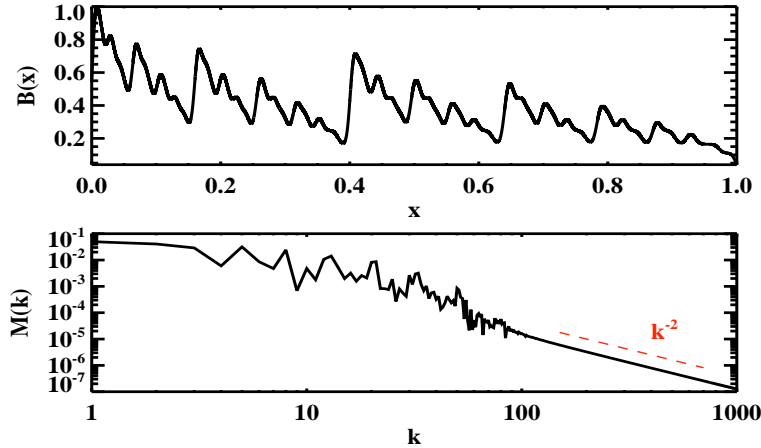


FIGURE 10. In the top panel, we show the eigenfunction  $B(x)$  for a 2-strip map dynamo for  $R_M = 10^6$ . In the bottom panel, we show the corresponding power spectrum  $M(k)$ .

An interesting case is when we use a random initial seed field, instead of a uniform one. In the Fig. 9, we show the evolution of such a run, starting from top left to bottom right. It can be seen that as the run progresses, the initial random field with both positive and negative values changes to an eigenfunction which is entirely negatively valued. This is clear on noting that the zero on the ordinate axis rapidly moves up showing that  $B(x)$  becomes more and more negative as it latches on to the eigenfunction. The  $B(x)$  in the bottom rightmost panel in Fig. 9 is the same eigenfunction as  $Rm = 1000$  case is Fig. 7, but with a negative amplitude. It could as well have become entirely positively valued depending on the initial seed field. This example also illustrates the fact that the eigenfunction of the map is realised independent of the initial conditions.

### 4.3. Fourier Analysis of the magnetic field

We can also calculate the Fourier series for  $B(x)$  to study the distribution of the magnetic power on different scales. The Fourier series is given by,

$$\tilde{B}(k) = \int_0^1 B(x) e^{-2\pi i x k} dx \quad (4.1)$$

where,  $k$  is wavenumber conjugate to  $x$ . Then the magnetic power spectrum can be defined as  $M(k) = |\tilde{B}(k)\tilde{B}^*(k)|/2$ .

In the Fig. 10, we show  $M(k)$  corresponding to the eigenfunction  $B(x)$  resulting from the two-strip map dynamo with  $R_M = 10^5$ . The log-log plot does not show  $M(k)$  for  $k = 0$  which holds a significant amount of total power. However in the given context, the  $k = 0$  component is just an overall constant factor in the eigenfunction and we would instead like to focus on the distribution of the power on smaller scales. We find that  $M(k)$  is non-smooth and can vary sharply within adjacent values of  $k$ . This is due to the fractal nature of the eigenfunction,  $B(x)$ . For fractal functions, several intermediate co-efficients in their Fourier series are expected to be zero (Korner 1988).

Note that  $M(k)$  at large  $k$ , follows as  $1/k^2$ . This is because at large  $k$ , the sines and cosines in Eq. 4.1 would sample a nearly constant part of  $B(x)$  (or a ramp function in this case). And the Fourier transform of the ramp function is  $\propto 1/k^2$ . In figures 11,13 and 17, we show  $M(k)$  for both two-strip and four-strip cases for different  $R_M$  in kinematic

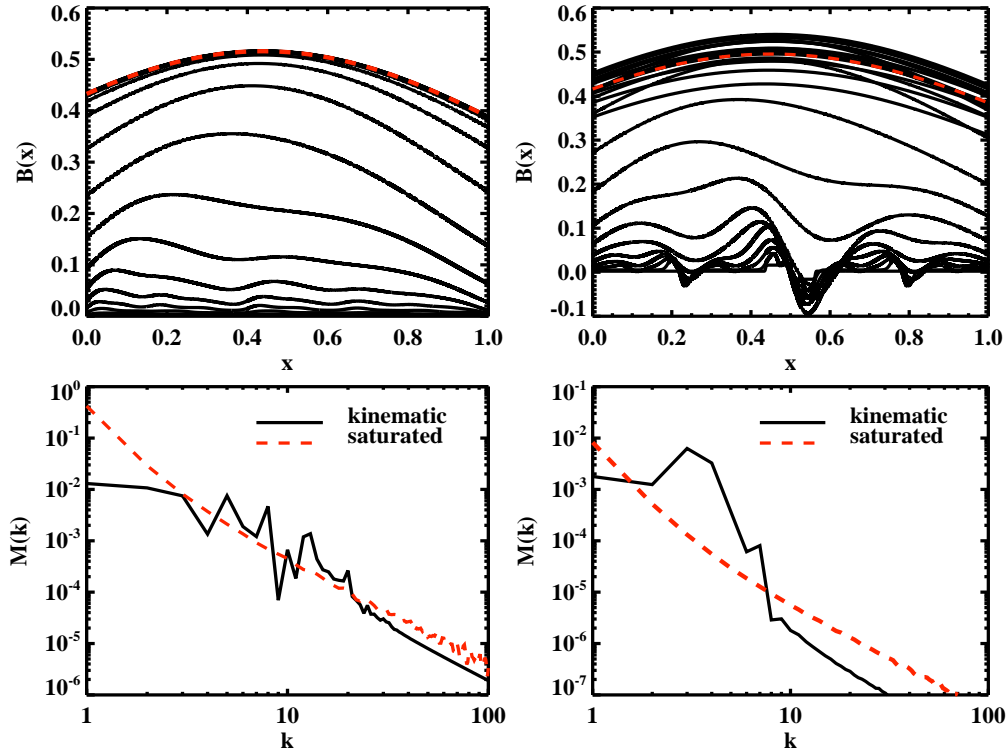


FIGURE 11. The nonlinear evolution of  $B(x)$ , due to saturation by increasing resistivity. The top left panel shows 2-strip map evolution adopting  $\alpha = 0.4$  and initial  $R_M = 10^4$ . The top right panel shows 4-strip map evolution with  $\alpha = \delta = 7/16$ ,  $\beta = \gamma = 1/16$  and initial  $R_M = 10^6$ . We see that the eigenfunction in both cases is driven to that of the marginal eigenfunction corresponding to  $R_M = R_{\text{crit}}$  on saturation. The bottom two panels show the magnetic power spectrum,  $M(k)$ , for the two cases respectively. The bold black line shows  $M(k)$  in kinematic regime and the red dashed line is the saturated case.

stage and compare it to the saturated one. We will say more about these figures below in the following section.

## 5. Saturation of STF map dynamos

Saturation of dynamos can occur in several different ways. Possibilities include the renormalization and increase of the effective resistivity due to Lorentz forces (Subramanian 1999) or the decreased stretching efficiency (Schekochihin *et al.* 2004). We model these in simple ways below to study the saturation of the map dynamos. We will now set the absolute value of the saturated magnetic field strength to be of order unity, and therefore start with an initial seed field of  $10^{-4}$ .

### 5.1. Saturation by decreasing $R_M$

As one possibility, consider saturating the dynamo by nonlinear increase of the effective resistivity as in the ambipolar drift model of Subramanian (1999). In this model as the magnetic field grows and Lorentz forces become important, the effective resistivity becomes  $\eta = \eta_0 + \tau B_{rms}^2 / 4\pi\rho$ . Here  $\eta_0$  is the microscopic resistivity,  $\tau$  is a response time,  $\rho$  is the fluid density and  $B_{rms}$  the rms value of  $|\mathbf{B}|$ . Multiplying and dividing the second term in  $\eta$  by  $v^2$ , where  $v$  is the rms turbulent velocity, we can rewrite this

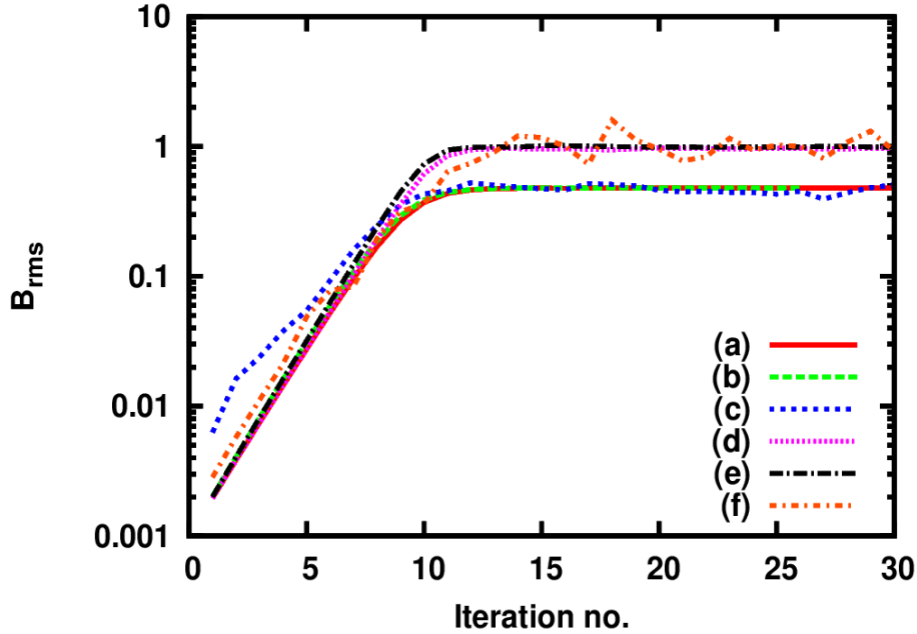


FIGURE 12. Comparison of  $B_{rms}$  for various cases, (a): 2 strip map with  $R_M = 1000$ , saturation by decreasing  $R_M$ , (b): 2 strip map with  $R_M = 10^4$ , saturation by decreasing  $R_M$ , (c): 4 strip map with  $R_M = 10^6$ , saturation by decreasing  $R_M$ , (d): 2 strip map with  $R_M = 1000$ , saturation by decreasing stretching, (e): 2 strip map with  $R_M = 10^4$ , saturation by decreasing stretching, (f): 4 strip map with  $R_M = 1000$ , saturation by decreasing stretching

as  $\eta = \eta_0(1 + R_{M0}B_{rms}^2/B_{eq}^2)$ , where  $R_{M0} = v^2\tau/\eta_0$  and  $B_{eq}^2 = 4\pi\rho v^2$ . Thus  $\eta_0/\eta = R_M/R_{M0} = (1 + R_{M0}B_{rms}^2/B_{eq}^2)^{-1}$ . We adopt such a picture for the map dynamo as well and model the nonlinear effect of the growing field by varying  $R_M$  at every iteration as,

$$R_M = \frac{R_{M0}}{1 + R_{M0}B_{rms}^2}. \quad (5.1)$$

Again  $R_{M0}$  is the initial value of  $R_M$  for the map and  $B_{rms}^2$  is now the average value of  $B^2(x)$  at any iteration (or time), taken to be normalised to the equipartition value.

This form models the possible increase of the renormalized resistivity due to Lorentz forces.

The time evolution of  $B(x)$  is shown in the left and right panels of Fig. 11 for 2-strip,  $R_{M0} = 10^4$  and 4-strip,  $R_{M0} = 10^6$  respectively. The evolution of corresponding  $B_{rms}$  is shown in Fig. 12 as case (a) and case (c) respectively. We see from Fig. 12 that  $B_{rms}$  indeed saturates after about 7 – 10 iterations, to a value of order unity. Moreover, on comparing left panel of Fig. 11 with left panel of Fig. 4 and right panel of Fig. 11 with right panel of Fig. 4, it is clear that the function  $B(x)$  representing the saturated state, is of the same form as  $B(x)$  for the critical  $R_M$  ( $\sim 4.35$ ). Further in the saturated stage the  $R_M$  given by the Eq. 5.1, also settles to  $R_{sat} = R_{crit} \sim 4$ , using  $B_{rms} \sim 0.5$  and  $R_{M0} = 1000$ .

In Fig. 11, we also show the corresponding magnetic power spectrum,  $M(k)$ , where the solid black curve is from the kinematic stage and the red dashed line is for the saturated field. It can be seen that the kinematic field exhibits peaks on smaller scales, around  $k \sim 5 - 20$  in 2-strip case and  $k \sim 3 - 10$  in the 4-strip case. The peaks seen on smaller

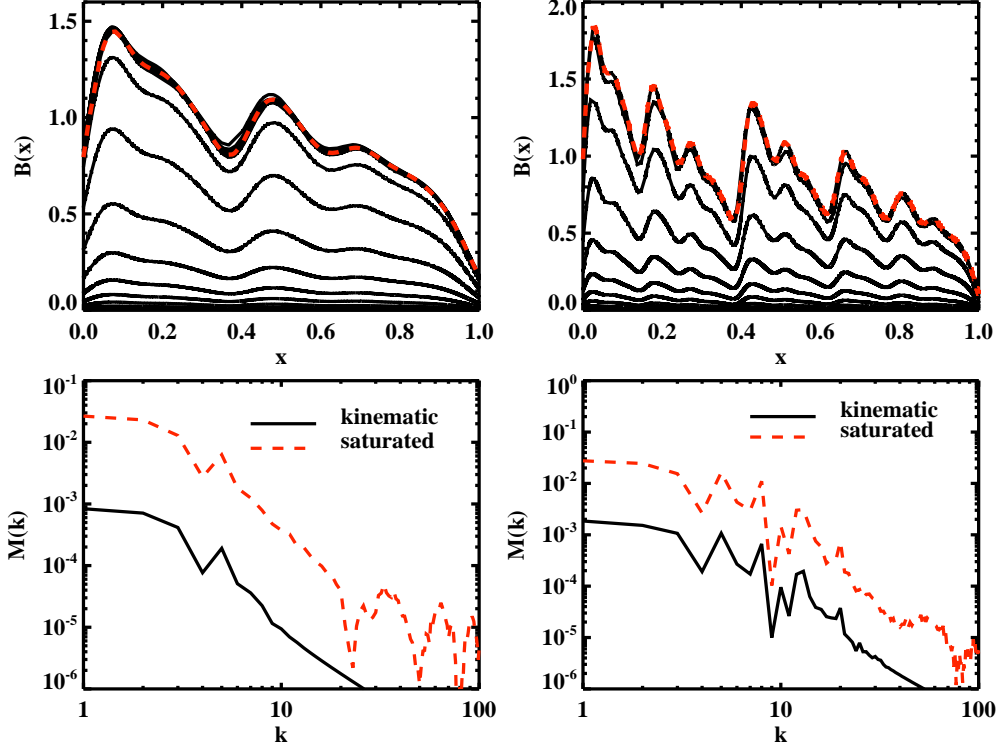


FIGURE 13. The nonlinear evolution of  $B(x)$  of the 2-strip map, due to saturation by reduced stretching, adopting initial  $\alpha_0 = 0.4$  and  $R_M = 1000$  (left top panel) and  $R_M = 10^4$  (right top panel). The red dashed line show  $B(x)$  in saturated state. The bottom two panels show the magnetic power spectrum,  $M(k)$ , for the two cases respectively. The bold black line shows  $M(k)$  in kinematic regime and the red dashed line is the saturated case.

scales (or larger  $k$ ) in kinematic stage seem to be smoothed out by saturation with an increase in the power in  $k \sim 1-2$ . Note that in both stages, however, the maximum power is in  $k = 0$  constant component, which does not appear in such a log-log plot. Thus in the case where saturation is obtained by renormalization of  $R_M$ , we find that the saturated state has the same spatial structure as the marginal state of the kinematic map dynamo. Such a result is similar to the saturation behaviour obtained in Subramanian (1999) and perhaps in the simulations of Haugen *et al.* (2004) for the  $P_M = 1$  fluctuation dynamo.

## 5.2. Saturation by decreasing stretching

### 5.2.1. Without changing the map

As the magnetic field strength increases, the effect of the Lorentz force would be to make it more difficult to amplify the field by stretching. Therefore, another way to achieve saturation in the maps would be to decrease the field amplification factor  $\propto 1/\alpha$  as a function of  $B_{rms}$ . We model this effect by multiplying  $\alpha, \beta$  in Eq. 5.5 for the 2-strip map and  $\alpha, \beta, \gamma, \delta$  in Eq. 3.6 for the 4-strip map by  $(1 + B_{rms}^2)$ . For example we adopt

$$\alpha = \alpha_0(1 + B_{rms}^2), \quad (5.2)$$

where  $\alpha_0$  is the initial value of  $\alpha$ . Note that to begin with we still leave the mapping of  $(x_n, y_n) \rightarrow (x_{n+1}, y_{n+1})$  described by Eqs. 5.3, 5.4, 3.4 and 3.5 as before, described by the initial  $\alpha_0, \beta_0, \gamma_0$  and  $\delta_0$ . Thus the unit square in the  $x - y$  plane is still mapped to

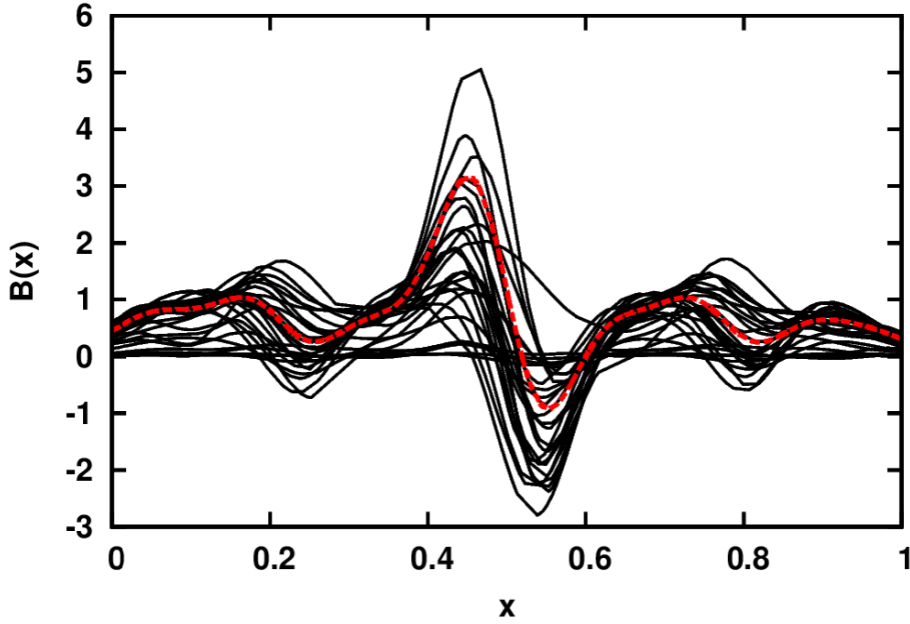


FIGURE 14. Same as in Fig. 13 but now for the 4-strip map adopting an initial  $\alpha_0 = \delta_0 = 7/16, \beta_0 = \gamma_0 = 1/16$  and  $R_M = 1000$ . The eigenfunction on saturation oscillates with a structure similar to the kinematic eigenfunction. The shape of kinematic eigen function is shown in dashed (red) line.

the unit square, but the amplification by stretching becomes progressively inefficient as  $B_{rms}$  grows.

Note that as one reduces stretching by a factor  $f_0 = 1/(1 + B_{rms}^2)$  and applies the STF map to a flux tube, its final radius  $R$  would decrease by  $f_0$  while its cross sectional area  $A$  would increase by  $1/f_0$ . In principle the physical dimensions of the unit square that we use to represent the flux tube would then change accordingly and it will become a rectangle with its  $y$ -dimension (analogous to the length of the flux tube) reduced by  $f_0$  and  $x$  dimension (analogous to the cross sectional area of the flux tube) increased by  $1/f_0$ . However, we are thinking of the unit square used in the map as representing the normalised flux tube radius and the normalised cross-sectional area. It is in this sense that the unit square is mapped onto itself, even though the degree of stretching is reducing with the growth of the field. We also now do not change the value of  $R_M$  during the diffusive step.

The result of the such reduced stretching for the 2-strip map is shown in left and right top panels of Fig. 13 for  $R_M = 1000$  and  $R_M = 10^4$  respectively. The corresponding  $B_{rms}$ , whose evolution is shown in Fig. 12 as cases (d) and (e), saturates after about 10 iterations. It is clear from comparing Fig. 13 with Fig. 7, that the distribution  $B(x)$  representing the saturated state in this case retains the complex structure of the growing kinematic eigenfunction and is quite different from the case of saturation by increased resistivity. It is thus not the marginal eigenfunction. In Fig. 13, we also show the magnetic power spectrum  $M(k)$  in the bottom two panels. Here again we see peaks on small scales, at  $k \sim 6$  for  $R_M = 1000$  and  $k \sim 4 - 20$  for  $R_M = 10^4$ . The saturated spectrum here matches with the one in the kinematic stage. This saturation behaviour is similar to what is argued by Schekochihin *et al.* (2004) for the fluctuation dynamo with large  $P_M$ , that

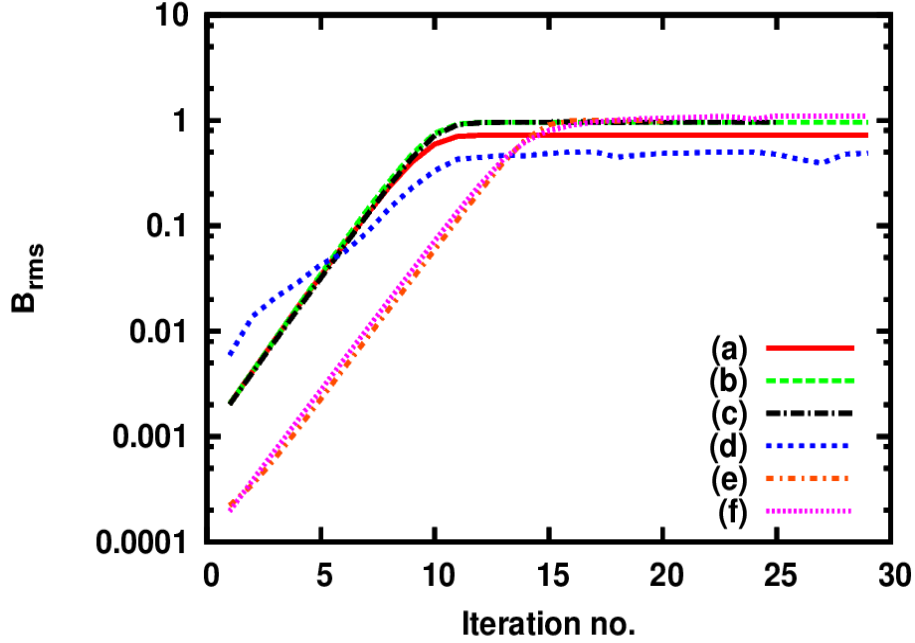


FIGURE 15. Comparison of  $B_{rms}$  for various cases, (a), (b), (c) and (d) show curves for saturation by combining decreasing both  $R_M$  and stretching. (a): 2 strip map with initial  $R_M = 10^6$ ,  $c_1 = 0.1$ ,  $c_2 = 0.9$ , (b): 2 strip map with initial  $R_M = 10^6$ ,  $c_1 = 0.001$ ,  $c_2 = 0.999$ , (c): 2 strip map with initial  $R_M = 10^4$ ,  $c_1 = 0.001$ ,  $c_2 = 0.999$ , (d): 4 strip map with initial  $R_M = 10^5$ ,  $c_1 = 0.001$ ,  $c_2 = 0.999$ , (e): 2 strip map with initial  $R_M = 10^3$ , saturation by decreasing stretching (by changing map), (f): 2 strip map with initial  $R_M = 10^3$ , saturation by decreasing stretching (by changing map) and also decreasing  $R_M$ , adopting  $c_1 = 0.1$  and  $c_2 = 0.9$ .

the field in the saturated state appears to be qualitatively similar to the growing field in the kinematic stage.

We have also employed a similar scheme for the 4-strip map with  $R_M = 1000$ . The results shown in Fig. 14 indicate a very different saturation behaviour. Now, the saturated eigenfunction  $B(x)$  oscillates with time although its form is similar to kinematic eigenfunction. Also  $B_{rms}$  oscillates about a steady value around unity, as can be seen in Fig. 12 (case (f)). This seems to indicate that if reversals are present, the saturated eigenfunction may never settle to a unique form.

### 5.2.2. Changing the map

On reduced stretching, as explained earlier, the physical dimensions of unit square map will change to become a rectangle. In the previous subsection, such a changed map is renormalised to unit square before the diffusion is carried out, thus effectively not changing the map. We now explore the consequences of renormalising the map to unit square only after the diffusion step; before we carry out further STF mapping. This renormalization process is to ensure that the next STF mapping can be done, as before, on a unit square. Such a modified mapping for the 2-strip case can be given as,

$$x_{n+1} = \begin{cases} \alpha_1 x_n & : y_n < \alpha; \\ \beta_1 x_n + \alpha_1 & : y_n > \alpha; \end{cases} \quad (5.3)$$

$$y_{n+1} = \begin{cases} y_n / \alpha_1 & : y_n < \alpha; \\ (y_n - \alpha) / \beta_1 & : y_n > \alpha; \end{cases} \quad (5.4)$$



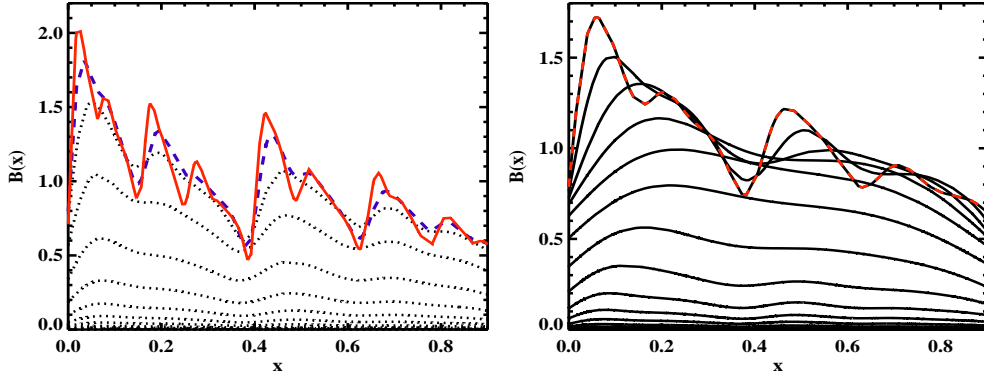


FIGURE 16. The evolution of  $B(x)$  in a 2-strip map dynamo,  $R_M = 1000$  in 2 cases. The left panel shows saturation by only reduced stretching with changed map. The last two iterations have been shown as dashed blue line and solid red line. And the right panel shows saturation by reduced stretching with changed map along with decreasing  $R_M$ , with  $c_1 = 0.1$  and  $c_2 = 0.9$ . The final iteration is shown in dashed red line.

The corresponding amplification of magnetic field in the region is given as:

$$B_{n+1}(x_{n+1}) = \begin{cases} B_n(x_n)/\alpha_2 & : x_n < \alpha_1; \\ B_n(x_n)/\beta_2 & : x_n > \alpha_1; \end{cases} \quad (5.5)$$

where initially, both  $\alpha_1$  and  $\alpha_2$  are  $\alpha_0$ . After the diffusion step, once we evaluate the current  $B_{rms}$ , we estimate  $\alpha_1 = \alpha_1(1 + B_{rms}^2)$  and  $\alpha_2 = \alpha_0(1 + B_{rms}^2)$ .

This implies that we are effectively working with the rectangle, which gets elongated further and further as the dynamo progresses. In Fig. 16, the left panel shows the evolution of a 2-strip,  $R_M = 1000$  run with such a saturation mechanism. We can see that the last few iterations overlap indicating the onset of saturation. While the magnetic energy saturates as seen in Fig. 15 in curve (e), such a process eventually becomes unstable in  $B(x)$ . This is because as the run progresses, the map grows in  $x$ -direction and diminishes continuously in  $y$ -direction, thus making the diffusion step progressively inefficient. This tends to a scenario wherein the effective  $R_M$  for the map keeps increasing leading to the ideal case in Fig 3. The  $B(x)$  seems to acquire more and more structures, as can be seen in the final two curves in dashed blue and solid red in Fig. 16 (left panel), reflecting the scenario of growing effective  $R_M$ .

In the flux tube picture, the flux tube will keep thickening and simultaneously grow smaller in size (radius). But at some point, this process will have to stop when both dimensions become comparable. Of course, the other possibility is that when the field grows to sufficiently high values, the tension in the flux tube will not allow further twisting and folding. One way of implementing a suppression in twisting and folding is to stop the map when the  $B_{rms}$  exceeds a threshold and allow for only diffusion. Although we have not explicitly shown this here, we expect that the  $B(x)$  will freeze to its form when it first crosses the threshold in  $B_{rms}$  thus retaining some structures from the kinematic eigenfunction.

### 5.3. Saturation by combining decreasing both $R_M$ and stretching

We now consider the saturation of the STF map dynamo, when the effects of decreasing effective  $R_M$  (due to increasing renormalised resistivity) and decreasing stretching efficiency are combined. We model this by introducing efficiency parameters  $c_1$  and  $c_2$  into

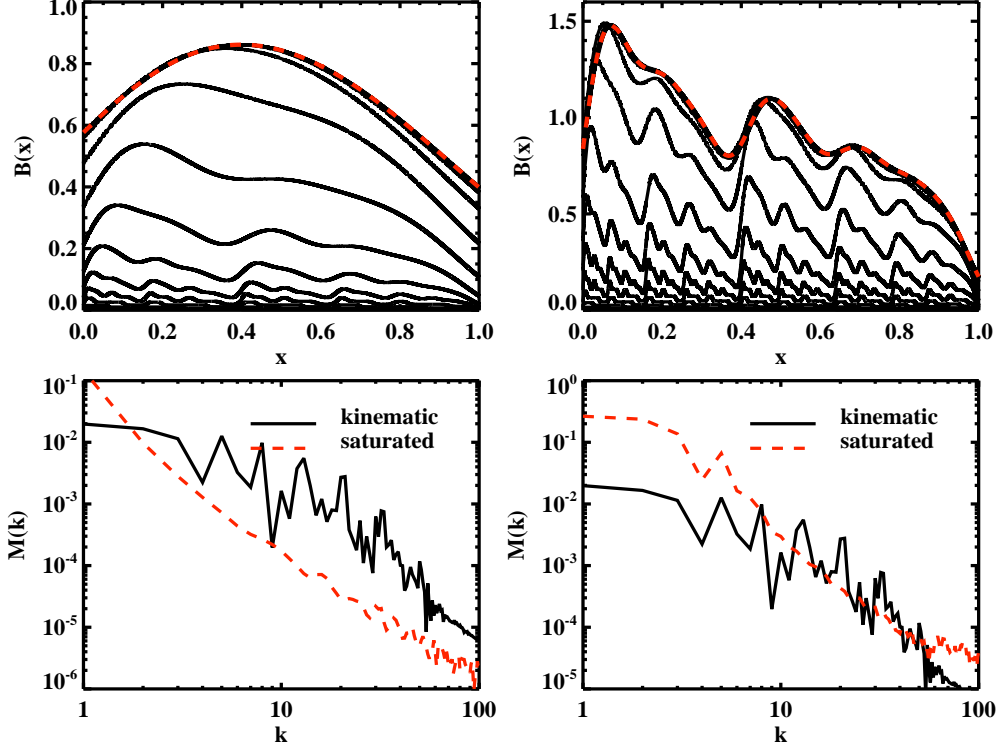


FIGURE 17. The nonlinear evolution of  $B(x)$  of the 2-strip map, due to saturation by combining both increased diffusion and reduced stretching (without changing the map), adopting initial  $\alpha_0 = 0.4$  and  $R_M = 10^6$ . The top left panel shows the result of adopting  $c_1 = 0.1$  and  $c_2 = 0.9$  (case A), while the top right panel shows the case when  $c_1 = 0.001$  and  $c_2 = 0.999$  (case B). The effective magnetic Reynolds number at saturation is  $R_{\text{sat}} = 18$  and  $R_{\text{sat}} = 1066$ , for case A and B respectively. The corresponding kinematic eigenfunctions are shown as dashed lines in the figure. We see that the shape of  $B(x)$  at saturation closely matches that of the kinematic eigenfunction for  $R_M = R_{\text{sat}}$ . The bottom two panels show the magnetic power spectrum,  $M(k)$ , for the two cases respectively. The bold black line shows  $M(k)$  in kinematic regime and the red dashed line is the saturated case.

Eqs. 5.1 and 5.2. We adopt

$$R_M = \frac{R_{M0}}{1 + c_1 R_{M0} B_{rms}^2}, \quad \alpha = \alpha_0 (1 + c_2 B_{rms}^2). \quad (5.6)$$

For  $c_1 = 1$  and  $c_2 = 0$  we have saturation purely by the nonlinear decrease of  $R_M$ , while  $c_1 = 0$  and  $c_2 = 1$  corresponds to the case when saturation occurs purely due to reduced stretching. We consider now the intermediate case where both  $c_1$  and  $c_2$  are non zero.

The evolution of  $B(x, t)$  of the 2-strip map, adopting initial  $\alpha_0 = 0.4$  and  $R_{M0} = 10^6$  is shown in Fig. 17, for two cases. The top left panel shows the result of adopting  $c_1 = 0.1$  and  $c_2 = 0.9$  (case A), while the top right shows the case when  $c_1 = 0.001$  and  $c_2 = 0.999$  (case B). The effective magnetic Reynolds numbers at saturation have now reduced from  $R_{M0} = 10^6$  to  $R_M = R_{\text{sat}} = 18$  and  $R_M = R_{\text{sat}} = 1066$ , for cases A and B respectively. The corresponding kinematic eigenfunctions are shown as dashed lines in the figure. Remarkably, we see from Fig. 17 that the the shape of  $B(x)$  at saturation for both cases, now closely matches that of the corresponding kinematic eigenfunction for  $R_M = R_{\text{sat}}$ . Thus when both the effective diffusion of the field and the stretching efficiency are affected

by Lorentz forces, as would perhaps be most realistic, then the dynamo saturates with an intermediate spatial structure; that of the kinematic eigenfunction with  $R_M = R_{\text{sat}}$  with  $R_{M0} > R_{\text{sat}} > R_{\text{crit}}$ .  $R_{\text{sat}}$  is determined by the relative importance of the increased diffusion versus the reduced stretching. However a change in  $c_1$  has a more dramatic effect than an equal change in  $c_2$ , as  $c_1$  appears in an exponential function, the Gaussian in Eq. 3.7 involved in convolution to incorporate resistive effects. In Fig. 15, we show saturation levels of the two runs in curves (a) and (b), which are close to a value of order unity. We also show the curve (c) for a run with lower  $R_M = 10^4$  which saturates to a similar level.

We also show the magnetic power spectrum,  $M(k)$ , in the bottom two panels in Fig. 17. For the case A, the saturated spectrum is smooth and increases monotonically towards smaller  $k$ . In case B, the saturated spectrum seems to still retain some peaks near  $k \sim 5$  and is flatter near  $k \sim 1-3$ , unlike case A. Thus reflecting the nature of field as expected for their corresponding lower and higher  $R_{\text{sat}}$  of 18 and 1066, respectively.

In the 4-strip map dynamo, this kind of saturation mechanism, with co-efficients,  $c_1 = 0.001$  and  $c_2 = 0.999$ , leads to large oscillations in the form of  $B(x)$  similar to the case when the saturation was only by reduced stretching. The field gets quite ordered by saturation as a result of inclusion of the mechanism increased resistivity even though the value of  $c_1$  is very small. These oscillations are also reflected in the evolution curve of  $B_{rms}$  in the Fig. 15 in curve (d).

Finally, we have also considered a case where we combine the two saturation mechanisms and at the same time change the map. The resulting  $B(x)$  evolution is shown in the right panel of the Fig. 16 adopting  $c_1 = 0.1$  and  $c_2 = 0.9$ , with  $R_M = 1000$ , for a 2-strip map dynamo. Compared to the case in the left panel in Fig. 16,  $B(x)$  saturates to a smoother kinematic eigenfunction, but then, the diffusion becomes less and less important, causing the field to develop finer scale structures, while its rms value still maintains a steady state as seen in curve (f) of Fig.15.

## 6. Conclusions

We have explored here the evolution and saturation behaviour of map dynamos used by Finn & Ott (1988, 1990) to model Zeldovich's STF dynamo. One of our aims is to use these simpler systems to develop some intuitive understanding of the saturation behaviour of more realistic fluctuation dynamos. The use of maps also allows one to analyze dynamos with very high values of  $R_M$ , much higher than what can be achieved in DNS.

We have considered in particular two types of the generalized Baker's maps, the 2-strip map where there is constant constructive folding and the 4-strip map which allows the possibility of reversal of the field. In the absence of diffusion, the magnetic field  $B(x)$  generated by the map dynamo develop fractal structures (Finn & Ott 1988, 1990). On including a diffusive step in the map, parameterised by the magnetic Reynolds number  $R_M$ , we find that the magnetic field  $B(x)$  latches on to an eigenfunction of the map dynamo and is amplified, only above a critical  $R_M = R_{\text{crit}} \sim 4$  for both types of dynamos. The spatial structure of the growing  $B(x)$  also becomes shape invariant (with iteration number), but whose complexity increases with increasing  $R_M$ . Such an eigenfunction is obtained independent of the initial field configuration, as we illustrated with an initial random seed field. The kinematic eigenfunction of the 4-strip map shows reversals of the field, whose number increases with  $R_M$ . These results are similar to those presented in Finn & Ott (1988, 1990) on the kinematic stage of the map dynamos, wherever the comparisons can be made. We have also illustrated both the kinematic and saturated

structure of  $B(x)$  by considering its power spectrum  $M(k)$ . In the kinematic case, the fractal nature of  $B(x)$  till the diffusive scale is reflected in sharp peaks in  $k$ -space.

We then explored different ways by which the STF map dynamos could saturate. Saturation can occur due to a renormalized increase of the effective resistivity or by decreasing  $R_M$ . Such an effect obtains in a model where the Lorentz forces leads to a ‘ambipolar’-type nonlinear drift velocity (Subramanian 1999). For both the 2-strip map and the 4-strip map which includes field reversals,  $B(x)$  in the saturated state goes back to the marginal eigenfunction, which would obtain for the critical  $R_M = R_{\text{crit}}$ . The structure developed during the kinematic stage is lost on saturation and thus one can conclude that the energy is being effectively transferred to the larger scales due to non-linear evolution as can also be seen from their power spectra. This is analogous to the analytical results of Subramanian (1999) and the DNS results of Haugen *et al.* (2004); Eyink *et al.* (2013); Bhat & Subramanian (2013) for fluctuation dynamos with  $P_M = 1$ .

We have also explored the saturation of the dynamo, when the effect of Lorentz forces is to decrease the efficiency of field amplification by stretching. This is implemented in two ways, (i) by not changing the map and (ii) when the map is changed to reflect the decreasing physical length (radius) of the flux tube and its increasing thickness.

For the 2-strip map, in case (i), we show that  $B(x)$  now saturates preserving the structure of the kinematic eigenfunction got using the initial  $R_M = R_{M0}$ .

In the case (ii), where we implement reduced stretching in the map, the magnetic energy (or  $B_{rms}$ ) saturates, but but the fractal structures in  $B(x)$  keep growing as in the ideal limit. Thus energy is still preserved at the smallest scales which survive resistive diffusion. This is analogous to the results of Schekochihin *et al.* (2004) for the large  $P_M$  and small  $Re$  fluctuation dynamo, where power on resistive scales appear to be preserved during saturation. However an intermediate behaviour obtains when both saturation mechanisms operate in tandem. The saturated  $B(x)$  has now the spatial structure of kinematic eigenfunction with an intermediate  $R_M = R_{\text{sat}}$  where  $R_{M0} > R_{\text{sat}} > R_{\text{crit}}$ . Even a small increase in the effective diffusion with growing field, (with  $c_1 \ll 1$ ) significantly smoothens the spatial structure of the field. For the 4-strip map, saturation due to decreased stretching efficiency with or without increased diffusion leads to a more complicated behaviour, as now the saturated  $B(x)$  oscillates with time, although with a structure similar to the kinematic eigenfunction.

One could have naively expected that  $B(x)$  is driven to a universal form on saturation. However, it appears that the field structure when dynamos saturate is a nontrivial issue even for the simple map dynamos, and depends on the exact manner of saturation. The two natural possibilities, that the saturated eigenfunction approaches the marginal eigenfunction or remains of the same form as the kinematic eigenfunction, are both realized for different modes of saturation. If one takes a hint from such map dynamos, then even for the fluctuation dynamo in a random flow, the structure of the saturated state could depend on the control parameters of the system, like  $R_M$ ,  $Re$  and  $R_{\text{crit}}$ . It would be interesting to explore such issues further. It would also be interesting to extend the map dynamos to incorporate a range of length scales, so as to mimic more realistically a turbulent flow with a range of eddy scales, and study their saturation behaviour.

## Acknowledgments

AS thanks IUCAA for hospitality during his visits there under the Visiting Student Programme. PB acknowledges support from CSIR. We acknowledge the use of the high performance computing facility at IUCAA. We thank two referees for useful comments

which has led to many improvements in the paper and Prof. A. D. Gangal for sharing his thoughts on the Fourier analysis of fractals.

## REFERENCES

- BERNET, M. L., MINIATI, F., LILLY, S. J., KRONBERG, P. P. & DESSAUGES-ZAVADSKY, M. 2008 Strong magnetic fields in normal galaxies at high redshift. *Natur* **454**, 302–304.
- BHAT, P. & SUBRAMANIAN, K. 2013 Fluctuation dynamos and their Faraday rotation signatures. *MNRAS* **429**, 2469–2481.
- BHAT, P. & SUBRAMANIAN, K. 2014 Fluctuation Dynamo at Finite Correlation Times and the Kazantsev Spectrum. *ApJ* **791**, L34.
- BRANDENBURG, A., SOKOLOFF, D. & SUBRAMANIAN, K. 2012 Current Status of Turbulent Dynamo Theory. From Large-Scale to Small-Scale Dynamos. *SSRv* **169**, 123–157.
- BRANDENBURG, A. & SUBRAMANIAN, K. 2005 Astrophysical magnetic fields and nonlinear dynamo theory. *PhR* **417**, 1–209.
- CHILDRESS, S. & GILBERT, A. D. 1995 *Stretch, Twist, Fold*.
- CHO, J. & RYU, D. 2009 Characteristic Lengths of Magnetic Field in Magnetohydrodynamic Turbulence. *ApJ* **705**, L90–L94.
- CLARKE, T. E. 2004 Faraday Rotation Observations of Magnetic Fields in Galaxy Clusters. *Journal of Korean Astronomical Society* **37**, 337–342.
- CLARKE, T. E., KRONBERG, P. P. & BÖHRINGER, H. 2001 A New Radio-X-Ray Probe of Galaxy Cluster Magnetic Fields. *ApJ* **547**, L111–L114.
- ENSSLIN, T. A. & VOGT, C. 2006 Magnetic turbulence in cool cores of galaxy clusters. *A&A* **453**, 447–458.
- EYINK, G., VISHNIAC, E., LALESCU, C., ALUIE, H., KANOV, K., BÜRGER, K., BURNS, R., MENEVEAU, C. & SZALAY, A. 2013 Flux-freezing breakdown in high-conductivity magnetohydrodynamic turbulence. *Natur* **497**, 466–469.
- EYINK, G. L. 2011 Stochastic flux freezing and magnetic dynamo. *PRE* **83** (5), 056405.
- FINN, J. M. & OTT, E. 1988 Chaotic flows and magnetic dynamos. *Physical Review Letters* **60**, 760–763.
- FINN, J. M. & OTT, E. 1990 The fast kinematic magnetic dynamo and the dissipationless limit. *Physics of Fluids B* **2**, 916–926.
- HAUGEN, N. E., BRANDENBURG, A. & DOBLER, W. 2004 Simulations of nonhelical hydromagnetic turbulence. *PRE* **70** (1), 016308.
- HAUGEN, N. E. L., BRANDENBURG, A. & DOBLER, W. 2003 Is Nonhelical Hydromagnetic Turbulence Peaked at Small Scales? *ApJ* **597**, L141–L144.
- KAZANTSEV, A. P. 1968 Enhancement of a Magnetic Field by a Conducting Fluid. *Soviet Journal of Experimental and Theoretical Physics* **26**, 1031.
- KORNER, T. W. 1988 *Fourier Analysis*. Cambridge University Press, Cambridge Books Online.
- MOLCHANOV, S. A., RUZMAIKIN, A. A. & SOKOLOV, D. D. 1984 A dynamo theorem. *Geophysical and Astrophysical Fluid Dynamics* **30**, 241–259.
- SCHEKOCHIHIN, A. A. & COWLEY, S. C. 2006 Turbulence, magnetic fields, and plasma physics in clusters of galaxies. *Physics of Plasmas* **13** (5), 056501.
- SCHEKOCHIHIN, A. A., COWLEY, S. C., TAYLOR, S. F., MARON, J. L. & MCWILLIAMS, J. C. 2004 Simulations of the Small-Scale Turbulent Dynamo. *ApJ* **612**, 276–307.
- SUBRAMANIAN, K. 1999 Unified Treatment of Small- and Large-Scale Dynamos in Helical Turbulence. *Physical Review Letters* **83**, 2957–2960.
- SUBRAMANIAN, K., SHUKUROV, A. & HAUGEN, N. E. L. 2006 Evolving turbulence and magnetic fields in galaxy clusters. *MNRAS* **366**, 1437–1454.
- TOBIAS, S. M., CATTANEO, F. & BOLDYREV, S. 2011 MHD Dynamos and Turbulence. *ArXiv e-prints*.
- VAINSHTEĪN, S. I. & ZEL'DOVICH, Y. B. 1972 REVIEWS OF TOPICAL PROBLEMS: Origin of Magnetic Fields in Astrophysics (Turbulent "Dynamo" Mechanisms). *Soviet Physics Uspekhi* **15**, 159–172.
- ZELDOVICH, I. B., RUZMAIKIN, A. A. & SOKOLOV, D. D., ed. 1983 *Magnetic fields in astrophysics*, vol. 3.

ZELDOVICH, Y. B., RUZMAIKIN, A. A. & SOKOLOFF, D. D. 1990 *The almighty chance*.